Apodization of imaging systems by means of a random spatially nonstationary absorbing screen

Marek Kowalczyk*

Departamento de Optica, Universitat de València, 46100 Burjassot, Spain

Pedro Andrés

Departamento de Ciencias Experimentales, Universitat Jaume I, 12080 Castellon, Spain

Manuel Martínez-Corral

Departamento de Optica, Universitat de València, 46100 Burjassot, Spain

Received November 25, 1991; accepted April 4, 1992; revised manuscript received April 13, 1992

The amplitude impulse response (AIR) of coherent imaging systems with random binary apodizers is analyzed. Formulas for the mean value and the variance of the AIR are derived for two statistical one-dimensional models of apodizers: (1) nonuniform low-density shot noise and (2) a nonuniform unipolar synchronous random process. We show that for both models a high signal-to-noise ratio is achieved within the central peak and the low-order sidelobes of the AIR. Apodizers based on the second model permit higher values of the signal-to-noise ratio than those based on the first one.

1. INTRODUCTION

There exists a large variety of methods of producing apodized pupils with continuously varying transmittance.[1] It is evident that the generation of such pupils is burdened with technical difficulties. Therefore attention has been paid recently to binary pupils, which in many coherent systems successfully substitute for the continuous ones.[1-3] Hegedus[4] has found that the most convenient way of producing a binary diffuser is to print equal-sized dots (e.g., with a light plotter) on a random carrier. In his method the average number of dots per unit area varies according to the pupil function. In Ref. 4 Hegedus has also proposed a simple algorithm that drives a printing device.[5] The problem of random binary elements in the pupil was also considered by Varamit and Indebetouw[6] and Beal and George.[7]

In this paper we analyze the amplitude impulse response (AIR) of a coherent imaging system with a random binary apodizer in the pupil plane. We derive expressions for the average and the variance of the AIR. We consider two models of random apodizers. The first is the model based on a nonuniform linearly filtered Poisson impulse process (nonuniform shot noise), and the second, that of Hegedus, may be classified as a nonuniform checkerboard model.

2. THEORY

For simplicity we assume the one-dimensional $4f$ imaging system with coherent illumination shown in Fig. 1. The finite bandwidth of the system is represented by a uniform pupil of width $2L$ placed in the spatial frequency plane. The transfer function of the system is given by

$$P(\nu) = \mathrm{rect}(\nu\lambda f/2L) = \mathrm{rect}(x/2L), \tag{1}$$

where λ is the wavelength of the illuminating beam, ν stands for spatial frequency, and x is the spatial coordinate in the spatial frequency plane. The amplitude transmittance of a randomly apodized pupil, $t(x)$, is assumed to be a sample function of a random spatially nonstationary process $T(x)$ whose values belong, in general, to the $(0,1)$ interval. We take into account the finite bandwidth of the system [Eq. (1)] by choosing the average value $\overline{t(x)}$ equal to zero for $|x| > L$ rather than by multiplying $t(x)$ by $P(x/2L)$. This seems to be reasonable in the case of a nonnegative process $T(x)$. For $|x| \le L$ we choose $\overline{t(x)}$ equal (at least approximately) to the deterministic apodized pupil function $p(x)$ that we intend to replace with a random, in particular, binary, function. We assume that $p(x)$ is real and symmetric.

Random Absorbing Pupil Modeled with Nonuniform Shot Noise of Low Density

Here we assume that $t(x)$ consists of a multitude of positive impulses $h(x - x_i)$ $(i = 1, 2, \ldots, N)$ of width l and unit height, which are distributed according to the Poisson law (see Fig. 2):

$$t(x) = h(x) \otimes \sum_{i=1}^{N} \delta(x - x_i), \tag{2a}$$

$$\mathrm{Prob}\{k \text{ impulses fall within the } (x_1, x_2) \text{ interval}\} = \frac{1}{k!}\left[\int_{x_1}^{x_2} \Lambda(x)\mathrm{d}x\right]^k \exp\left[-\int_{x_1}^{x_2} \Lambda(x)\mathrm{d}x\right], \tag{2b}$$

where $\otimes$ is the convolution operation, δ is a Dirac delta function, N is the number of impulses on the whole real axis, and $\Lambda(x)$ is the rate function of the Poisson impulse process. $\Lambda(x)$ is assumed to be a Fourier-transformable

0740-3232/92/111930-07$05.00

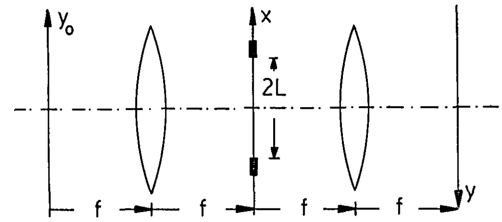

Fig. 1. Geometry of the one-dimensional $4f$ imaging system.

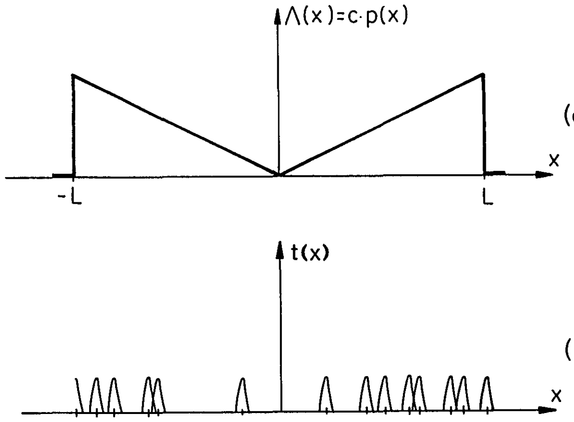

Fig. 2. Example of the nonuniform shot-noise process. (a) Rate function $\Lambda(x) = c|x|/L$ for $|x| \leq L$ and zero otherwise; (b) sample function corresponding to the rate function in (a).

function and equal to zero for $|x| > L$; therefore

$$\int \Lambda(x)\mathrm{d}x = \int_{-L}^{L} \Lambda(x)\mathrm{d}x = \overline{N}. \tag{3}$$

We put

$$\Lambda(x) = cp(x), \tag{4}$$

where c is a dimensional constant in inverse meters. By a proper choice of the value of c we can avoid the overlap of the impulses $h(x - x_i)$. Consequently, the real amplitude transmittance $t(x)$ given by Eqs. (2) is kept in the (0, 1) interval. This is the case (with high probability) when the condition

$$\Lambda(x)l \leq 0.5 \tag{5}$$

holds, i.e., when we deal with so-called low-density shot noise.[8] If the condition of inequality (5) is fulfilled, the probability that more than one impulse falls within the interval $(x, x + l)$ is equal to at most 0.09. Assuming maximum values of $p(x) = 1$ and $l = 50$ μm, inequality (5) will be fulfilled if $c \leq 1/2l = 10^4\ \mathrm{m}^{-1}$. The impulse $h(x)$ is assumed to be the impulse response of a certain linear and space invariant system. In Fig. 3 we show a negative of the random absorbing screen whose rows represent the sample functions of the form given by Eqs. (2) [multiplied by $\mathrm{rect}(x'/l)$, where x' is the spatial coordinate in the pupil plane perpendicular to x]. In Fig. 3 we put the rate function $\Lambda(x)$ in the form presented in Fig. 2(a) for two different values of c.

The average pupil function $\overline{t(x)}$ is given by[9]

$$\overline{t(x)} = \Lambda(x) \otimes h(x) = cp(x) \otimes h(x). \tag{6}$$

Thus $\overline{t(x)}$ is approximately proportional to $p(x)$ only if

$$l \ll L. \tag{7}$$

For $h(x) = \mathrm{rect}(x/l)$ and $c = 1/2l$ we have

$$\overline{t(x)} = c\int p(\zeta)\mathrm{rect}\left(\frac{x-\zeta}{l}\right)\mathrm{d}\zeta = c\int_{x-l/2}^{x+l/2} p(\zeta)\mathrm{d}\zeta = \frac{1}{2l}\int_{x-l/2}^{x+l/2} p(\zeta)\mathrm{d}\zeta. \tag{8}$$

If l is sufficiently small, $p(x)$ may be considered a linear function within any interval of the length l, and so

$$\overline{t(x)} = 0.5p(x). \tag{9}$$

It is seen that the use of the low-density shot-noise model causes a double suppression of the dynamic range of pupil function. This effect can be observed in Fig. 3, where both edges of the negative of the filter (corresponding to the transmittance of the positive's being equal to unity) are not filled up with black dots.

The average impulse response of the imaging system shown in Fig. 1 above is given by[10]

$$\bar{s}\left(\frac{y}{\lambda f}\right) = \overline{\frac{1}{\lambda f}\int t(x)\exp\left(-\frac{2\pi i}{\lambda f}yx\right)\mathrm{d}x} = \frac{1}{\lambda f}\int \overline{t(x)}\exp\left(-\frac{2\pi i}{\lambda f}yx\right)\mathrm{d}x. \tag{10}$$

From Eqs. (6) and (10) and the convolution theorem, it holds that

$$\bar{s}\left(\frac{y}{\lambda f}\right) = \frac{Ll}{\lambda f}\mathcal{L}\left(\frac{Ly}{\lambda f}\right)\mathcal{H}\left(\frac{ly}{\lambda f}\right) = \frac{Llc}{\lambda f}\mathcal{P}\left(\frac{Ly}{\lambda f}\right)\mathcal{H}\left(\frac{ly}{\lambda f}\right), \tag{11}$$

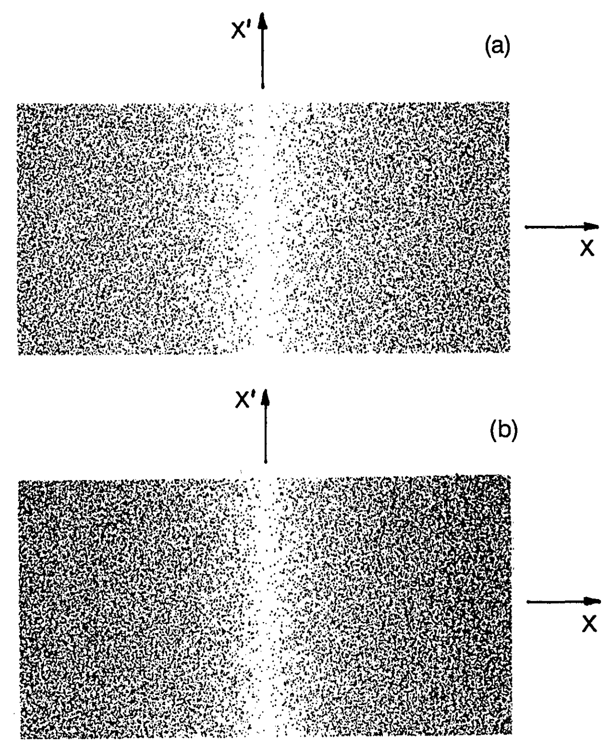

Fig. 3. Negatives of absorbing screens based on nonuniform shot noise. Each row represents a sample function of the form given by Eqs. (2) multiplied by $\mathrm{rect}(x'/l)$. The rate function $\Lambda(x)$ is put in the form presented in Fig. 2(a) for two values of c: (a) $c = 25\ \mathrm{mm}^{-1}$, (b) $c = 50\ \mathrm{mm}^{-1}$. In both cases $l = 0.017$ mm (150 dots per inch) and $L = 50$ mm.

where $\mathscr{L}$, $\mathscr{H}$, and $\mathscr{P}$ are the Fourier transforms of Λ, h, and p, respectively. Therefore $(L/\lambda f)\mathscr{P}(Ly/\lambda f)$ is the AIR of the system with the pupil function $p(x)$, and $l\mathscr{H}(ly/\lambda f)$ is the transfer function of the system that forms impulses $h(x - x_i)$. It can be the system such as that shown in Fig. 1 with the object transparency whose amplitude transmittance equals

$$O(y_0) = \sum_{i=1}^{N} \delta(y_0 - y_{0i}). \tag{12}$$

If such a system is sufficiently defocused, i.e., the image registration plane does not coincide with the geometrical image plane, the impulse response of the system has an approximately rectangular (binary) form.[11] Of course, in practice we print finite-sized dots at random points [Eqs. (2)] with a light plotter rather than use an imaging system with an object that consists of a set of point sources. Nevertheless, interpretation of $\mathscr{H}$ as a transfer function is useful in a spectral analysis of random pupil functions. In particular, well-known results of a spectral analysis of nonuniform shot noise can be invoked.[12]

We assume that the relation given by expression (7) holds; therefore, in the neighborhood of the central maximum of $\mathscr{P}(Ly/\lambda f)$, the function $\mathscr{H}(ly/\lambda f)$ is approximately constant. Hence the average AIR $\bar{s}$ is proportional to the impulse response $\mathscr{P}$ of our interest. For $h(x) = \text{rect}(x/l)$ and $cl = 0.5$, Eq. (11) yields

$$\bar{s}\left(\frac{y}{\lambda f}\right) = \frac{L}{2\lambda f}\mathscr{P}\left(\frac{Ly}{\lambda f}\right)\text{sinc}\left(\frac{ly}{\lambda f}\right) \approx \frac{L}{2\lambda f}\mathscr{P}\left(\frac{Ly}{\lambda f}\right). \tag{13}$$

In order to calculate the variance $\sigma_s^2(y)$ of the impulse response $s(y)$, we use the definition of the variance of a complex random process:

$$\sigma_s^2(y) = \overline{|s(y) - \overline{s(y)}|^2}. \tag{14}$$

Since for symmetric $p(x)$ the average impulse response $\overline{s(y)}$ is real, Eq. (14) yields the following variance:

$$\sigma_s^2(y) = \overline{|s(y)|^2} - [\overline{s(y)}]^2. \tag{15}$$

The first term on the right-hand side of Eq. (15) is proportional to the energy spectral density of the process $T(x)$, whose sample functions are those given by Eqs. (2) above. Thus this term equals[12]

$$\overline{|s(y)|^2} = \left(\frac{Ll}{\lambda f}\right)^2 \mathscr{L}^2\left(\frac{Ly}{\lambda f}\right)\mathscr{H}^2\left(\frac{ly}{\lambda f}\right) + \left(\frac{l}{\lambda f}\right)^2 \overline{N}\mathscr{H}^2\left(\frac{ly}{\lambda f}\right). \tag{16}$$

Equations (11), (15), and (16) yield

$$\sigma_s^2(y) = \left(\frac{l}{\lambda f}\right)^2 \overline{N}\mathscr{H}^2\left(\frac{ly}{\lambda f}\right) \approx \left(\frac{l}{\lambda f}\right)^2 \overline{N}. \tag{17}$$

The narrower the impulses $h(x - x_i)$, the smaller the variance of $s(y)$ and the better the above approximation. The signal-to-noise ratio (SNR) in the point-source image given by a coherent system with randomly apodized pupil may be defined as

$$\text{SNR}(y) = |\overline{s(y)}|/\sigma_s(y). \tag{18}$$

Although the SNR defined above cannot be measured directly in an experiment, as it refers to amplitude but not to intensity distribution, it can be a useful parameter when the behaviors of various types of random apodizer in a coherent imaging system are compared. Equations (11), (17), and (18) yield

$$\text{SNR}(y) = L|\mathscr{L}(Ly/\lambda f)|\overline{N}^{-1/2}. \tag{19}$$

In order to obtain the correct form of the dependence of SNR(y) on $\overline{N}$, we must take into account the fact that the function $\mathscr{L}$, being the Fourier transform of the rate function Λ, also depends on $\overline{N}$. We can express this dependence explicitly by introducing a normalized Fourier transform of Λ:

$$\hat{\mathscr{L}}(Ly/\lambda f) = \frac{\mathscr{L}(Ly/\lambda f)}{\mathscr{L}(0)}. \tag{20}$$

Since

$$L\mathscr{L}\left(\frac{Ly}{\lambda f}\right) = \int \Lambda\left(\frac{x}{L}\right)\exp\left(-\frac{2\pi i}{\lambda f}yx\right)\mathrm{d}x, \tag{21}$$

then

$$\mathscr{L}(0) = \frac{1}{L}\int \Lambda\left(\frac{x}{L}\right)\mathrm{d}x = \frac{\overline{N}}{L}. \tag{22}$$

It follows from Eqs. (19), (20), and (22) that

$$\text{SNR}(y) = \overline{N}^{1/2}|\hat{\mathscr{L}}(Ly/\lambda f)| = \overline{N}^{1/2}|\hat{\mathscr{P}}(Ly/\lambda f)|, \tag{23}$$

where $\hat{\mathscr{P}}(y) = \mathscr{P}(y)/\mathscr{P}(0)$ is the normalized AIR of the imaging system with the deterministic pupil function $p(x)$.

Equations (17) and (23) show that the variance of the noise component in the point-source image is approximately constant (independent of y) and affects first the sidelobes and not the central maximum, where a high SNR is achieved. Therefore the pupil function generated with the nonuniform shot-noise model is suitable for superresolution and maximum energy concentration within the central peak.

Random Absorbing Pupil Modeled with a Unipolar Synchronous Nonstationary Random Process

A one-dimensional analog of the checkerboard model used by Hegedus is a unipolar synchronous nonstationary random process (random nonstationary unipolar binary transmission) described below. Say that we are given a sequence of points x_n such that

$$x_n = e + nl, \qquad n = 0, \pm 1, \pm 2, \tag{24}$$

where e is a random variable uniformly distributed in the $(-l/2, l/2)$ interval. We construct a random pupil function $t(x)$ as follows: for each point x_n from the $(-L, L)$ interval, if

$$\text{RND}(n) \leq p(x_n), \tag{25}$$

then at x_n a rectangular impulse of unit height and width l is localized; if otherwise, then $t(x) = 0$ in the interval $(x_n - l/2, x_n + l/2)$. RND(n) is a random number uniformly distributed in the $[0, p_{\max}(x)]$ interval and generated for the point x_n. We assume that $p(x)$ is normalized in such a way that $p_{\max}(x) = 1$. Thus $t(x)$ is of the form (see Fig. 4)

$$t(x) = \sum_k \text{rect}\left(\frac{x - x_{n_k}}{l}\right) = \sum_k \text{rect}\left[\frac{x - (e + n_k l)}{l}\right], \tag{26}$$

where x_{n_k} are those x_n for which inequality (25) is met. For such sample functions the values $t(x_n)$ and $t(x_m)$ are

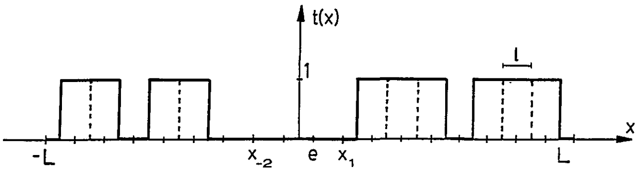

Fig. 4. Example of the unipolar synchronous nonstationary random process; $e = l/2$, $p(x_n) = |x_n|/L$ for $x_n \leq L$ and zero otherwise.

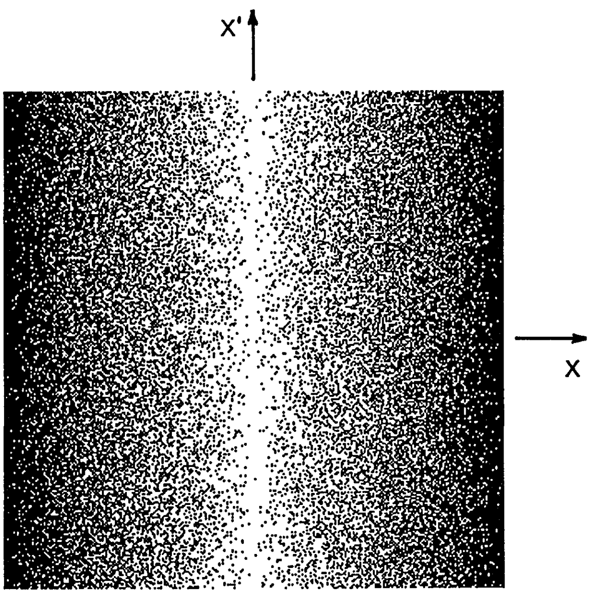

Fig. 5. Negative of absorbing screen based on the unipolar synchronous nonstationary random process for e and $p(x_n)$ as in Fig. 4; $l = 0.034$ mm, $L = 50$ mm.

statistically independent ($m \neq n$). In Fig. 5 we show a negative of the random absorbing screen whose rows are the sample functions given by Eq. (26) multiplied by $\mathrm{rect}(x'/l)$. For each sample we put $e = l/2$ and $p(x) = |x|/L$ for $|x| \leq L$ and zero otherwise.

To proceed further, we assume that l is small enough that we may consider $p(x)$ to be linear within any interval of length l. First we calculate the average pupil function $\overline{t(x)}$. To this end, we need to take into account the statistics of the random variables e and RND. We calculate $\overline{t(x)} \triangleq E[t(x)]$, using the concept of conditional mean value[13]:

$$E[t(x; e, \mathrm{RND})] = E_e\{E_{\mathrm{RND}|e}[t(x; e, \mathrm{RND}) \,|\, e = e_0]\}$$
$$= E_e\{E_{\mathrm{RND}|e}[t(x; e_0, \mathrm{RND}) \,|\, e = e_0]\}, \quad (27)$$

where E_e and E_{RND} denote averaging over e and RND, respectively. We can choose e_0 in such a way that x will be one of the points x_n. If so, then

$$E_{\mathrm{RND}}[t(x; e_0, \mathrm{RND}) \,|\, e = e_0]$$
$$= 1 \cdot \mathrm{Prob}\{\mathrm{RND}(n) \leq p(x = x_n)\}$$
$$+ 0 \cdot \mathrm{Prob}\{\mathrm{RND}(n) > p(x = x_n)\}$$
$$= 1 \cdot p(x_n) + 0 \cdot [1 - p(x_n)] = p(x_n). \quad (28)$$

Since e is uniformly distributed within the $(-l/2, l/2)$ interval, the cell to which point x belongs may be centered (with equal probability) at any point in the interval $(x - l/2, x + l/2)$. Thus

$$E[t(x; e, \mathrm{RND})] = E_e[p(x - e)]$$
$$= \frac{1}{l} \int \mathrm{rect}\left(\frac{e}{l}\right) p(x - e)\mathrm{d}e$$
$$= \frac{1}{l}\,\mathrm{rect}\left(\frac{x}{l}\right) \otimes p(x)$$
$$= \frac{1}{l} \int_{x-l/2}^{x+l/2} p(\zeta)\mathrm{d}\zeta \approx p(x). \quad (29)$$

The above approximation holds owing to our assumption on the linearity of $p(x)$ in any interval of length l.

Comparison of Eqs. (9) and (29) shows that the model investigated in this subsection conserves the dynamics of pupil function, whereas the low-density shot-noise model does not.

Using Eqs. (10) and (29), we obtain the average impulse response

$$\bar{s}\left(\frac{y}{\lambda f}\right) = \frac{L}{\lambda f}\mathcal{P}\left(\frac{Ly}{\lambda f}\right)\mathrm{sinc}\left(\frac{ly}{\lambda f}\right)$$
$$= \frac{l\overline{M}}{\lambda f}\hat{\mathcal{P}}\left(\frac{Ly}{\lambda f}\right)\mathrm{sinc}\left(\frac{ly}{\lambda f}\right) \approx \frac{l\overline{M}}{\lambda f}\hat{\mathcal{P}}\left(\frac{Ly}{\lambda f}\right), \quad (30)$$

where $\overline{M} = \overline{\int t(x)\mathrm{d}x/l} = L\mathcal{P}(0)/l$ is the average number of transparent cells.

To evaluate the variance of $s(y)$, we first calculate explicitly the first term on the right-hand side of Eq. (15) above:

$$\overline{|s(y)|^2} = \left(\frac{1}{\lambda f}\right)^2 \iint \overline{t(x_1)t(x_2)\exp\left[-\frac{2\pi i}{\lambda f}(x_1 - x_2)y\right]\mathrm{d}x_1\mathrm{d}x_2}$$
$$= \left(\frac{1}{\lambda f}\right)^2 \iint R(x_1, x_2)\exp\left[-\frac{2\pi i}{\lambda f}(x_1 - x_2)y\right]\mathrm{d}x_1\mathrm{d}x_2, \quad (31)$$

where $R(x_1, x_2)$ is the autocorrelation function of the process whose sample functions are those given above by Eq. (26).

We calculate $R(x_1, x_2)$ following the method presented in Ref. 14 for the random stationary checkerboard absorbing screen. Some necessary modifications are introduced owing to the lack of stationarity in our case. Since different cells have statistically independent values of transmittance, the autocorrelation function can be written as

$$R(x_1, x_2) = \overline{t(x_1)t(x_2)}$$
$$= E^{[1,2]}[t(x_1)t(x_2)]\mathrm{Prob}\begin{Bmatrix} x_1 \text{ and } x_2 \text{ are in} \\ \text{the same cell} \end{Bmatrix}$$
$$+ \overline{t(x_1)t(x_2)}\ \mathrm{Prob}\begin{Bmatrix} x_1 \text{ and } x_2 \text{ are in} \\ \text{different cells} \end{Bmatrix}. \quad (32)$$

Here $E^{[1,2]}[t(x_1)t(x_2)]$ denotes statistical average of the product $t(x_1)t(x_2)$ for such pairs (x_1, x_2) for which x_1 and x_2 belong to the same cell. Again, taking into account the statistics of RND and e, we obtain the following for x_1 and x_2 in the same cell:

$$E^{[1,2]}[t(x_1)t(x_2)]$$
$$= E_e^{[1,2]}\{E_{\mathrm{RND}}^{[1,2]}[t(x_1)t(x_2); e_0, \mathrm{RND} \,|\, e = e_0]\}. \quad (33)$$

Since

$$E_{\mathrm{RND}}^{[1,2]}[t(x_1)t(x_2); e_0, \mathrm{RND}\,|\, e = e_0] = 1^2 \cdot p\left(\frac{x_1 + x_2}{2}\right) + 0^2 \cdot \left[1 - p\left(\frac{x_1 + x_2}{2}\right)\right], \quad (34)$$

we have

$$E^{[1,2]}[t(x_1)t(x_2)] = \frac{1}{l - (x_1 - x_2)} \int_{-[l-(x_1-x_2)]/2}^{[l-(x_1-x_2)]/2} p\left(\frac{x_1 + x_2}{2} - e\right) \mathrm{d}e \approx p\left(\frac{x_1 + x_2}{2}\right). \quad (35)$$

To calculate Eq. (33), we chose e_0 in such a way that the point $(x_1 + x_2)/2$ coincided with a certain point x_n. Then we noticed that, if the points x_1 and x_2 were to be kept in the same cell, e could vary only in the interval $[-l/2 + (x_2 - x_1), l/2 - (x_2 - x_1)]$.

We have that

$$\mathrm{Prob}\begin{Bmatrix} x_1 \text{ and } x_2 \text{ are in} \\ \text{the same cell} \end{Bmatrix} = \Delta\left(\frac{x_1 - x_2}{l}\right), \quad (36)$$

where $\Delta(x) = 1 - |x|$ for $|x| \leq 1$ and zero otherwise. It follows that

$$R(x_1, x_2) = p\left(\frac{x_1 + x_2}{2}\right)\Delta\left(\frac{x_1 - x_2}{l}\right) + p(x_1)p(x_2)\left[1 - \Delta\left(\frac{x_1 - x_2}{l}\right)\right]. \quad (37)$$

Equations (31) and (37) yield

$$\begin{aligned}\overline{|s(y)|^2} = \left(\frac{1}{\lambda f}\right)^2 \Bigg\{ &\iint p\left(\frac{x_1 + x_2}{2}\right)\Delta\left(\frac{x_1 - x_2}{l}\right) \times \exp\left[-\frac{2\pi i}{\lambda f}(x_1 - x_2)y\right]\mathrm{d}x_1\mathrm{d}x_2 \\ &+ \iint p(x_1)p(x_2)\exp\left[-\frac{2\pi i}{\lambda f}(x_1 - x_2)y\right]\mathrm{d}x_1\mathrm{d}x_2 \\ &- \iint p(x_1)p(x_2)\Delta\left(\frac{x_1 - x_2}{l}\right) \times \exp\left[-\frac{2\pi i}{\lambda f}(x_1 - x_2)y\right]\mathrm{d}x_1\mathrm{d}x_2\Bigg\}. \end{aligned} \quad (38)$$

It follows from Eqs. (15), (30), and (38) that

$$\begin{aligned}\sigma_s^2(y) = \left(\frac{1}{\lambda f}\right)^2 \Bigg\{ &\iint p\left(\frac{x_1 + x_2}{2}\right)\Delta\left(\frac{x_1 - x_2}{l}\right) \times \exp\left[-\frac{2\pi i}{\lambda f}(x_1 - x_2)y\right]\mathrm{d}x_1\mathrm{d}x_2 \\ &- \int p(x_1)\mathrm{d}x_1 \int p(x_2)\Delta\left(\frac{x_1 - x_2}{l}\right) \times \exp\left[-\frac{2\pi i}{\lambda f}(x_1 - x_2)y\right]\mathrm{d}x_2\Bigg\}. \end{aligned} \quad (39)$$

We use the substitutions $x_1 + x_2 = \xi$, $x_1 - x_2 = \eta$ in the first double integral of Eq. (39). Then we apply the commutative law of convolution, the convolution and autocorrelation theorems, and the condition $L \gg l$ in the second double integral of Eq. (39). The result is

$$\sigma_s^2(y) = \left(\frac{1}{\lambda f}\right)^2 \left[l\,\mathrm{sinc}^2\left(\frac{ly}{\lambda f}\right) \int p(x)\mathrm{d}x - lL^2\,\mathrm{sinc}^2\left(\frac{ly}{\lambda f}\right) \int \mathcal{P}^2\left(\frac{Ly}{\lambda f}\right) d\left(\frac{y}{\lambda f}\right)\right]. \quad (40)$$

According to the Parseval theorem,

$$\int \mathcal{P}^2\left(\frac{Ly}{\lambda f}\right)\mathrm{d}y = \frac{\lambda f}{L^2} \int p^2(x)\mathrm{d}x.$$

Thus we have

$$\sigma_s^2(y) = \left(\frac{1}{\lambda f}\right)^2 l\,\mathrm{sinc}^2\left(\frac{ly}{\lambda f}\right)\left[\int p(x)\mathrm{d}x - \int p^2(x)\mathrm{d}x\right]. \quad (41)$$

Since $0 \leq p(x) \leq 1$ and, consequently, $p(x)$ is always of the same sign, the second law of the mean for integrals enables us to rewrite Eq. (41) as

$$\sigma_s^2(y) = \left(\frac{l}{\lambda f}\right)^2 \mathrm{sinc}^2\left(\frac{ly}{\lambda f}\right)(1 - \beta)\frac{1}{l}\int p(x)\mathrm{d}x, \quad (42)$$

where β fulfills the inequality $0 < \beta \leq 1$. The coefficient β is equal to the ratio of average (over the pupil) intensity transmittance to average amplitude transmittance:

$$\beta = \frac{\int p^2(x)\mathrm{d}x}{\int p(x)\mathrm{d}x} = \frac{\frac{1}{2L}\int_{-L}^{L} p^2(x)\mathrm{d}x}{\frac{1}{2L}\int_{-L}^{L} p(x)\mathrm{d}x}. \quad (43)$$

For the apodized pupil shown above in Fig. 2, we obtain $\beta = 2/3$. For the uniform pupil whose transmittance $p(x) = b\,\mathrm{rect}(x/2L)$, we have $\beta = b$. With $l^{-1}\int p(x)\mathrm{d}x = \overline{M}$ the variance is

$$\sigma_s^2(y) = \left(\frac{l}{\lambda f}\right)^2 \mathrm{sinc}^2\left(\frac{ly}{\lambda f}\right)\overline{M}(1 - \beta) \approx \left(\frac{l}{\lambda f}\right)^2 \overline{M}(1 - \beta). \quad (44)$$

Equations (18), (30), and (44) yield the SNR

$$\mathrm{SNR}(y) = \frac{\overline{M}^{1/2}}{(1 - \beta)^{1/2}}\left|\hat{\mathcal{P}}\left(\frac{Ly}{\lambda f}\right)\right|. \quad (45)$$

For $\overline{M} = 64$ and $\beta = 2/3$, Eq. (45) gives SNR(0) = 13.8. It follows from Eqs. (23) and (45) that the use of a random apodizer based on the checkerboard model yields higher values of the SNR by the factor of $(1 - \beta)^{-1/2}$ for $\overline{N} = \overline{M}$.

3. CONCLUSIONS

In Section 2 we presented two models of random binary apodizers that can easily be fabricated in a two-step process: (1) generation of a random binary pattern (negative) with a light plotter or a laser printer and (2) photographic reduction onto a high-resolution film (positive). We have related the average pupil function, the average AIR, and the SNR in the image of a point source to the following parameters of the binary pattern: the width and the average number of transparent cells and the integral transmittance of the pupil. We have shown that the smaller the size l of the transparent cell, the better the average transmittance of the randomly apodized pupil approximates the pupil function of an apodizer with continuously varying transmittance [Eqs. (8) and (29) above] and the better the average AIR approximates the corresponding deterministic AIR [Eqs. (13) and (30) above]. This means that, in order to generate the binary pattern, we should work near the resolution limit of our printing device. It should be pointed out that, irrespective of the relationship between the width of the impulse $h(x)$ and the width of the cell in the checkerboard model, the corresponding average pupil functions are equal up to a multiplicative constant resulting from the restriction given by inequality (5). This constant may be equal to at most 0.5 [Eq. (9) above]. Thus, for the low-density shot-noise model (realized by means of the two-step process mentioned above), the value of the average pupil function varies within the interval (0, 0.5). If the negative binary pattern were positive, the average pupil function would vary within the interval (0.5, 1). This means that the pupil function would contain quite a strong constant component. This can easily be seen from Fig. 3, in which negatives of linearly apodized superresolving pupils (with shaded central part) are shown.

We have shown that for $l \ll L$, which should be the case for a good random binary apodizer, the variance of the AIR in practice does not depend on spatial coordinates and is proportional to l^2 and to the average number of transparent cells [Eqs. (17) and (44) above]. For the checkerboard model the variance is also proportional to the factor $1 - \beta$. Therefore the larger the average transmittance, the smaller the variance.

As regards the SNR that characterizes the AIR of a randomly apodized imaging system, we have shown that this parameter is proportional to the square root of the average number of transparent cells ($\overline{N}$ or $\overline{M}$) and to the modulus of the normalized deterministic impulse response $\hat{\mathcal{P}}(Ly/\lambda f)$ [Eqs. (23) and (45) above]. As a result of its dependence on $\hat{\mathcal{P}}$, the SNR depends strongly on y and achieves relatively high values within the central peak and the low-order sidelobes of the AIR. It should be stressed that, in the case in which the width of the cells in the checkerboard model and the width of the impulses $h(x - x_i)$ are equal and $\Lambda(x)l = 0.5$ [inequality (5) above], the average number of impulses is $\overline{N} = \overline{M}/2$. Moreover, in Eq. (45) there is a factor of $(1 - \beta)^{-1/2} > 1$ that is absent in Eq. (23). Therefore the SNR that can be achieved for the checkerboard model is higher than that for the shot-noise model by the factor of $\sqrt{2}(1 - \beta)^{-1/2}$, which for $\beta = 1/2$ is equal to 2 (assuming in both cases the same resolution limit of the printing device, equal to $1/l$).

From our analysis it results that the stochastic nature of the presented apodizers affects, first, the high-order sidelobes of the AIR; therefore these apodizers can be useful for typical applications of apodization, where the shape of the central maximum is of importance.

The extension of our results to a two-dimensional model is straightforward. In the two-dimensional case, $\overline{M}$ plays the role of average total number of transparent cells. So a high SNR can be obtained for a relatively small linear dimension of the quadratic matrix of cells.

Further improvement of the SNR could be made by the application of methods that were developed for displaying continuous-tone images on bilevel displays, where values of transmittance (reflectance) in neighbor cells are usually correlated (e.g., error-diffusion method).[15] The results obtained for the two relatively simple models presented in this paper may serve as a lower limit of the SNR that could be achieved with more sophisticated methods, which are usually quite difficult to treat analytically.

We would like to point out that we are interested in finding the method that would enable us to reach the maximal resemblance (according to a certain criterion) of moduli of Fourier spectra of binarized and continuous apodizers and not the maximal visual resemblance of the underlying apodizers themselves. Thus our task is close to that of optimal binarization of computer-generated binary Fourier-transform holograms,[16] in which the methods developed for the binarization of continuous-tone images are widely used as well.[17]

ACKNOWLEDGMENTS

The authors are grateful to M. J. Yzuel for bringing to their attention the studies of Z. S. Hegedus and for encouragement of this research. This research was supported by the Dirección General de Investigación Científica y Técnica (grant PB 87-0617), Ministerio de Educación y Ciencia, Spain. Marek Kowalczyk acknowledges gratefully a grant from the Conselleria de Cultura, Educació i Ciència de la Generalitat Valenciana, Spain.

*Permanent address, Institute of Geophysics, University of Warsaw, Pasteura 7, 02 093 Warsaw, Poland.

REFERENCES AND NOTES

1. Z. S. Hegedus, "Annular pupil arrays. Application to confocal scanning," Opt. Acta **32,** 815–826 (1985), and references therein.
2. Z. S. Hegedus and V. Sarafis, "Superresolving filters in confocally scanned imaging systems," J. Opt. Soc. Am. A **3,** 1892–1896 (1986).
3. C. J. R. Sheppard and Z. S. Hegedus, "Axial behavior of pupil-plane filters," J. Opt. Soc. Am. A **5,** 643–664 (1988).
4. Z. S. Hegedus, "Pupil filters in confocal imaging," in *Confocal Microscopy,* T. Wilson, ed. (Academic, London, 1990), pp. 171–183.
5. There are some typographical errors in Ref. 4; therefore, for the benefit of the reader, we recall here this algorithm following the typescript of this reference: "...the negatives [...] were generated by the following simple algorithm:

```
for every point within the pupil
  if RND < |P|
    then draw a dot
    else move to the next point
```

Here RND is a random number and $P = P(\tau)$ is the desired pupil function. Both quantities are normalized."
6. C. Varamit and G. Indebetouw, "Imaging properties of defocused partitioned pupils," J. Opt. Soc. Am. A **2,** 799–802 (1985).
7. M. M. Beal and N. George, "Features in the optical transforms of serrated apertures and disks," J. Opt. Soc. Am. A **6,** 1815–1826 (1989).
8. A. Papoulis, *Probability, Random Variables, and Stochastic Processes* (McGraw-Hill, New York, 1965), p. 565.
9. Ref. 8, p. 433.
10. Ref. 8, p. 466.

11. J. W. Goodman, *Introduction to Fourier Optics* (McGraw-Hill, New York, 1968), p. 124.
12. J. W. Goodman, *Statistical Optics* (Wiley, New York, 1985), Sec. 3.7.4.
13. Ref. 8, p. 208.
14. Ref. 12, Sec. 8.2.2.
15. E. Peli, "Multiresolution, error-convergence halftone algorithm," J. Opt. Soc. Am. A **8**, 625–636 (1991), and references therein.
16. B. K. Jennison, J. P. Allebach, and D. W. Sweeney, "Efficient design of direct-binary-search computer-generated holograms," J. Opt. Soc. Am. A **8**, 652–660 (1991).
17. E. Bernard, "Optimal error diffusion for computer-generated holograms," J. Opt. Soc. Am. A **5**, 1803–1817 (1988).